

Near-infrared observations of galaxies in Pisces-Perseus

III. Global scaling relations of disks and bulges

G. Moriondo¹, R. Giovanelli², and M.P. Haynes²

¹ Dipartimento di Astronomia e Scienza dello spazio, Università di Firenze, L.E. Fermi 5, I-50125 Firenze, Italy

² Center for Radiophysics and Space Research, Cornell University, Ithaca, NY 14853, USA

Received 26 November 1998 / Accepted 29 March 1999

Abstract. We determine the parameters of scaling relations analogous to the Fundamental Plane of elliptical galaxies for the bulges and disks of a sample of 40 spiral galaxies. To this end we derive structural parameters (scalelengths and surface brightnesses) from near infrared H band images, and kinematical parameters (rotational velocities) from optical rotation curves. In the case of the disks, we test the accuracy of the derived relation as a distance indicator by comparing its scatter to that of the H band Tully–Fisher relation for the same sample, and find that the accuracy attained by the latter is slightly higher (the dispersion is 19% versus 23% for this sample). It is speculated that the difference is due to the more robust character of global parameters, rather than those associated with the inner parts of disks. It also appears that (a) either the stellar mass-to-light ratios of bulge and disk increase with the size of the components, or (b) the bulge and disk relative contributions to the overall rotation of the galaxy (and, as a consequence, to its total mass) become steadily smaller with increasing size.

Key words: galaxies: structure – galaxies: fundamental parameters – galaxies: distances and redshifts – infrared: galaxies

1. Introduction

The existence of tight scaling relations between observable photometric and kinematic galaxy parameters, in particular the Fundamental Plane (FP) of elliptical galaxies (Jørgensen et al. 1996, Scodreggio 1997), and the Tully-Fisher relation for spirals (TF, Tully & Fisher 1977), finds its most straightforward application in the evaluation of galaxy distances. The small scatter observed in both relations implies a fine tuning between parameters strictly related to the stellar component alone, such as the optical luminosity, and the kinematic properties of the galaxy, which are affected by the overall mass distribution (both dark and visible).

In the case of spiral galaxies, it is therefore suggestive that a tight scaling relation may also exist between photometric and kinematic properties *of the disks alone*, with a scatter as low as, or even lower, than the TF relation. Karachentsev (1989)

found that, for a sample of 15 edge-on galaxy, the disk scale length R_d was connected to the 21 cm line velocity width W and the I -band central disk brightness $I(0)$ by the relation $R_d \propto W^{1.4} I(0)^{-0.74}$, with a scatter in $\log(R_d)$ of 0.048. The uncertainty implied in the distance is around 12%, smaller than the one usually achieved by the TF relation (15 ~ 20%). More recently Chiba & Yoshii (1995, CY95 hereafter) tested on a sample of 14 nearby spirals the relation

$$\log R_d = a \log(V_2 I(0)^{-0.5}) + b \quad (1)$$

in the B band, where V_2 is the galaxy rotation velocity measured at 2.2 disk scalelengths. Since the contribution from the disk to the overall rotation curve (RC) has a maximum at this particular distance, the authors argue that the contributions from bulge and dark halo are likely to be less important, and therefore the measured velocity should represent a good estimate for the rotation of the disk alone. For a set of exponential disks of fixed mass-to-light ratio (M/L) one would expect $\log R_d \sim \log [V_2^2/I(0)]$, corresponding to $a = 2$ in Eq. (1). Actually CY95 find $a = 1.045$, again with a remarkably small scatter. On the other hand, recent work from Giovanelli (1997) suggests that the accuracy of Eq. (1) as a distance indicator is inferior to the one attained by the traditional TF relation by at least a factor of 2.

Besides being a tool to provide redshift-independent distances, scaling relations also contain information about how galaxies – and in particular their “visible” constituents – have formed and evolved (Gavazzi 1997, Ciotti 1997, Dalcanton et al. 1997, Burstein et al. 1997 – BBFN hereafter). In this respect, spiral disks are a potentially “easy” class of systems, since they are all characterized by well defined shape and kinematics: if the effects of extinction on their surface brightness distribution are accounted for, and a reliable estimate of their mass is obtained, the subsequent scaling relations will be directly related to systematic variations in the disks’ stellar content. Further information can be provided by the variation with wavelength of such properties, in particular by scaling relations involving colours (e.g., the colour magnitude relation; see Gavazzi 1993, Tully et al. 1998, Peletier & de Grijs 1998).

In this work we investigate the existence and tightness of a general scaling relation in the near infrared (NIR), similar to

the one defining the FP, for both structural components (disks and bulges) of a sample of 40 nearby spiral galaxies. Our aim is to test the power of these relations as tools to measure galaxy distances, and use them to provide new information about the stellar content and star formation history of spiral galaxies. In the present paper we are going to deal mainly with the problem of the distance measurements, leaving a thorough discussion of the second point to future work. The use of NIR photometry is well suited for a study of this kind, since it minimizes the effect of internal extinction, and provides a good tracing of the stellar mass. In most cases, high resolution, optical RC's allow us to trace the gravitational potential of the galaxies up to their innermost regions.

The photometric parameters are obtained, in the NIR H band, from a bi-dimensional decomposition of the galaxy images, as described in Sect. 3. In Sect. 4 we show how the kinematical information are extracted from the galaxy RC's, to which we fit a model composed by bulge, disk, and a dark halo. We subsequently derive the coefficients of the FP for bulges and disks, and compare the potential accuracy in a distance determination achieved by the disks' relation to the one we obtain using the TF relation for the same sample. We finally investigate the trends of M/L 's with luminosity and galaxy size. Throughout the paper we adopt a Hubble constant $H_0 = 75 \text{ km s}^{-1} \text{ Mpc}^{-1}$.

2. The data

The 40 spiral galaxies considered for this study are drawn from a larger sample selected in the Pisces-Perseus supercluster region, for which H band images are available (see Moriondo et al. 1998b and 1999 for a thorough description of the original sample). This subset in particular contains the galaxies for which a RC is also available both from the literature or the private database of RG and MH, and includes morphological types ranging from Sa to Scd. In most cases, the RC's are derived from optical emission lines measurements and are confined within two or three disk scale lengths. For a few galaxies radio aperture-synthesis RC's (21 cm HI line) are also available, extending well beyond the optical radius. All the RC's were rescaled to our adopted values of distance and inclination. For all the galaxies (except UGC 2885) 21 cm line velocity widths are also available from the database of RG and MH. We will use these values later on to derive the H band TF relation for the sample. Table 1 contains the basic information on the galaxies of the sample as well as the references for the RC's; many of these were retrieved from the compilations by Corradi & Capaccioli (1991) and Prugniel et al. (1998). We note that this sample is not appropriate to obtain an absolute calibration of distances. It is however well suited to compare two different scaling relations and their relative accuracy as distance indicators.

3. The fits to the brightness distributions

The photometric data reduction and analysis are described in detail in Moriondo et al. (1998a, 1999). Briefly, each galaxy

image is fitted with a model consisting of an exponential disk and a bulge, whose shape is described by a generalized exponential (Sèrsic 1968). Both brightness distributions are assumed to be elliptical in the plane of the sky, and with a common centre and major axis. The parameters of the fit are the two scalelengths, surface brightnesses and apparent ellipticities (one for each component). The results of these decompositions were used in Moriondo et al. (1998b) to evaluate the effect of internal extinction on the H -band structural parameters and derive the corrections to the face-on aspect. The corrected values for scalelengths, surface brightnesses and total luminosities will be used in the following analysis. In most cases an exponential bulge yields a satisfactory fit to the data. For two galaxies in the subsample considered here (namely UGC 26 and UGC 820), a value $n = 2$ of the "shape" parameter in the exponent of the bulge brightness distribution produces better results. In two cases (UGC 673 and UGC 975) the disk alone is sufficient to fit the galaxy, i.e. no trace of a bulge is found in the brightness distribution. Table 2 contains the photometric parameters of the sample galaxies, corrected to the face-on aspect and for the redshift; the H -band total luminosity, in Column 8, will be introduced in Sect. 5. The resulting decompositions are plotted in the top panels of Fig. 1, together with the surface brightness profiles averaged along elliptical contours (from Moriondo et al. 1999), and the brightness profiles along the major axis. In the case of UGC 673 and UGC 12666, the discrepancy between these two profiles is due to the ellipse-fitting routine, which in both cases has underestimated the galaxy apparent ellipticity in the regions of lower signal-to-noise ratio. Our fits, however, are in good agreement with the respective brightness distributions, so that the estimated parameters are reliable for these galaxies as well.

4. The fits to the rotation curves

To estimate the contribution of bulge and disk to a given RC we use the information from the photometric data to predict the shape of the RC's of the two components, and derive their M/L ratios from a best fit to the observed velocity profile. The accuracy of this technique, which has been used for a long time by many authors (van Albada et al. 1985, Kent 1986, Martimbeau et al. 1994, Moriondo et al. 1998c), is actually impaired by the scarce knowledge on the contribution of the dark component to the overall RC. This becomes certainly important beyond the disk rotation peak, at around two disk wavelengths; however, it might also be significant at smaller radii, especially for low luminosity and low surface brightness galaxies – as suggested by Persic et al. (1996) and de Blok & McGaugh (1997) – but also in the case of bright spirals (see Bosma, 1998, for a recent review on this topic). Courteau and Rix (1999) and Bottema (1993, 1997), for instance, estimate the disk contribution to be about 60% of the overall rotation at 2.2 scalelengths, whereas different authors (e.g. Verheijen & Tully 1998, Dubinski et al. 1999, Gerhard 1999, Bosma 1998) support a "maximum disk" scenario in which such contribution is about 85%, at least for bright galaxies. The shape of the dark matter distribution is

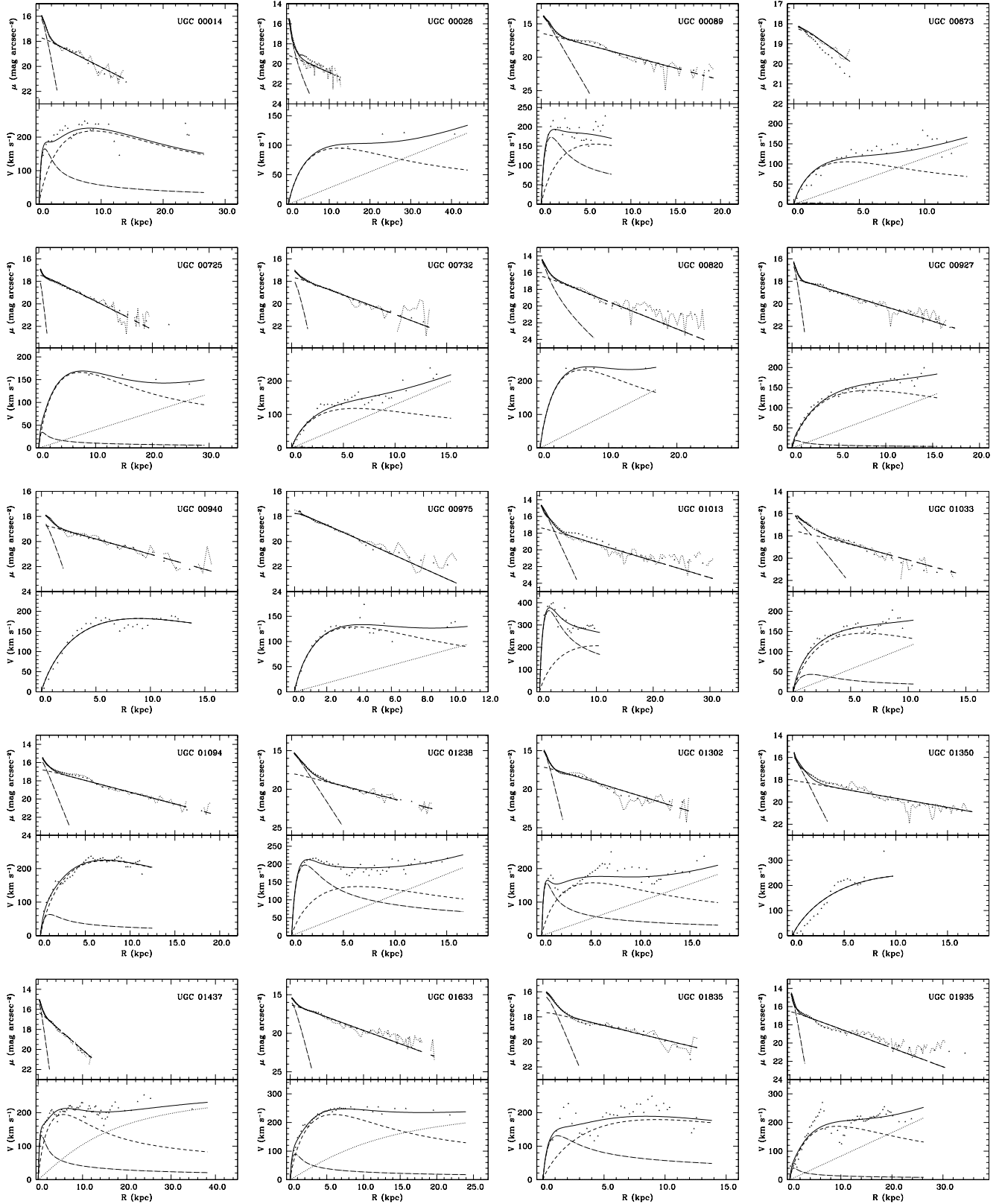


Fig. 1. Top panels: radial surface brightness profiles of the sample galaxies, in a magnitude scale. For each plot, the triangles represent the profile obtained by averaging the intensity over elliptical profiles (see Moriondo et al. 1999); the dotted line is a cut along the major axis of the galaxy; also shown are the best fit to the data (solid line) and the contributions from bulge (dot-dash line) and disk (dashed line). Bottom panels: the observed RC's (triangles) with the best fit to the data (solid line). Again, the dot-dash and dashed lines represent the contributions from bulge and disk respectively. The contribution from the dark halo is shown as a dotted line.

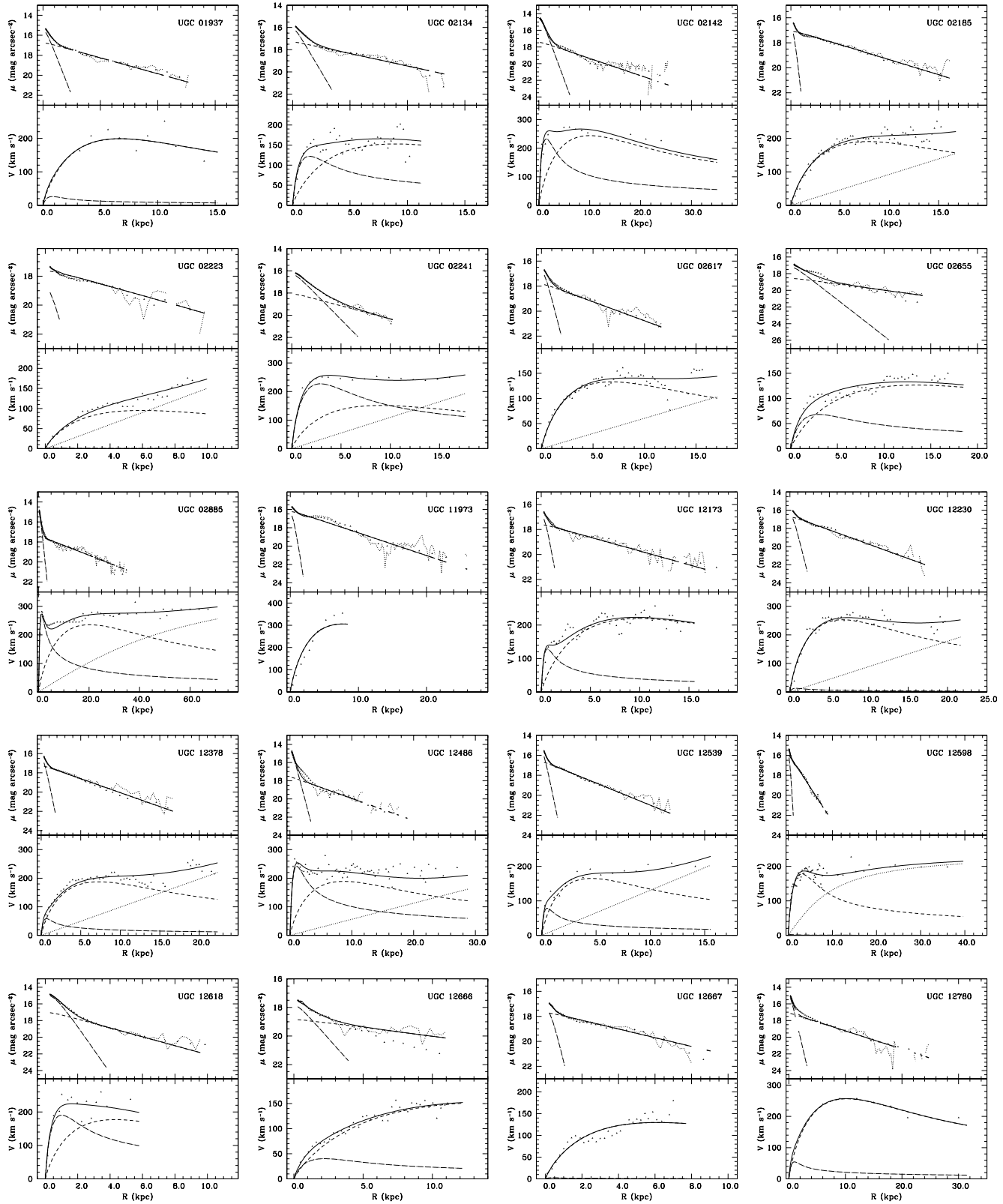


Fig. 1. (continued)

Table 1. The galaxy sample

Names (1) (2)	R.A. (J2000) (3)	Dec. (4)	RH Type (5)	m_B (6)	$P.A.$ (7)	D (Mpc) (8)	RC code (9)	
UGC 00014		00 03 35.0	23 12 03	Sc	13.8	41	92	1,2
UGC 00026	NGC 7819	00 04 24.5	31 28 19	SB(s)b	14.2	99	61	3
UGC 00089	NGC 0023	00 09 53.4	25 55 25	SB(s)a	12.8	171	56	4
UGC 00673		01 06 09.7	31 24 24	SAC?	15.7	45:	79	1
UGC 00725		01 10 11.0	43 06 35	SBcd?	14.4	47	63	5
UGC 00732		01 10 44.4	33 33 28	SA(r)d	14.6	81	68	1
UGC 00820	NGC 0452	01 16 14.8	31 02 01	SBab	13.6	35	62	6
UGC 00927	NGC 0496	01 23 11.5	33 31 46	Sbc	14.1	38	76	1,7
UGC 00940		01 23 37.9	34 34 11	SA(s)c	15.1	68	89	7
UGC 00975		01 25 15.6	34 21 34	S	15.0	123	61	7
UGC 01013	NGC 0536	01 26 21.6	34 42 14	SB(r)b	13.2	72	65	7
UGC 01033		01 27 34.9	31 33 16	Scd:	14.1	132	50	7
UGC 01094	NGC 0582	01 31 57.7	33 28 33	SB?	14.1	60	54	7
UGC 01238	NGC 0668	01 46 22.6	36 27 39	Sb	13.7	30	56	7,8
UGC 01302	NGC 0688	01 50 44.1	35 17 04	(R')SAB(rs)b	13.3	141	52	7,8
UGC 01350		01 52 57.5	36 30 47	SB(r)b	14.2	44	67	7
UGC 01437	NGC 0753	01 57 42.4	35 54 57	SAB(rs)bc	13.0	131	62	7,8,9,10
UGC 01633	NGC 0818	02 08 44.4	38 46 36	SABc:	13.2	114	53	9,11
UGC 01835	IC 0221	02 22 41.3	28 15 28	Sc	13.7	5:	65	1
UGC 01935	NGC 0931	02 28 14.5	31 18 42	Sbc	14.5	82	64	1,12
UGC 01937	NGC 0935	02 28 10.9	19 35 59	Scd:	13.6	153	52	13
UGC 02134		02 38 51.8	27 50 50	Sb	14.2	100	58	1
UGC 02142	NGC 1024	02 39 12.2	10 50 50	(R')SA(r)ab	13.1	158	44	14
UGC 02185		02 43 11.4	40 25 34	Scd:	13.5	141	55	1
UGC 02223		02 45 14.4	35 11 21	Scd:	14.8	46	63	1
UGC 02241	NGC 1085	02 46 25.3	03 36 26	SA(s)bc:	13.1	2	88	15
UGC 02617		03 16 00.7	40 53 08	SAB(s)d	13.8	10	59	7
UGC 02655		03 18 45.3	43 14 20	SAB(s)d	13.5	–	80	7
UGC 02885		03 53 02.4	35 35 22	SA(rs)c	13.5	45	76	10,16
UGC 11973		22 16 50.4	41 30 13	SAB(s)bc	12.9	42	52	17
UGC 12173		22 43 52.0	38 22 37	SAB(rs)c	13.5	101	59	1,7
UGC 12230	NGC 7407	22 53 21.2	32 07 44	Sbc	13.9	160	81	1
UGC 12378	NGC 7489	23 07 32.5	22 59 50	Sd	14.0	164	78	1
UGC 12486	NGC 7591	23 18 16.2	06 35 09	SBbc	13.9	167:	61	1,2,8,18
UGC 12539	NGC 7631	23 21 26.7	08 13 05	SA(r)b:	13.9	77	45	18
UGC 12598	NGC 7664	23 26 39.9	25 04 50	Sc:	13.4	88	42	1,10,19
UGC 12618	NGC 7679	23 28 46.8	03 30 41	SB0	13.5	–	64	20
UGC 12666		23 33 41.0	32 23 02	Scd:	14.4	124	62	1
UGC 12667		23 33 49.5	30 03 37	Scd:	13.5	127	46	1
UGC 12780	NGC 7753	23 47 04.7	29 29 01	SAB(rs)bc	12.8	71	64	21

Notes: Cols. 5,6: from the Third Reference Catalogue of Bright Galaxies (RC3), de Vaucouleurs et al. 1991. Col. 7: from Moriondo et al. 1999. Col. 9: references for the rotation curves. 1: Courteau 1992; 2: Mathewson et al. 1992; 3: Szomoru et al. 1994; 4: Afanas'ev 1988a; 5: Van Moorsel 1983; 6: Oosterloo & Shostak 1993; 7: Vogt 1995; 8: Amram et al. 1994; 9: Broeils & Van Woerden 1994; 10: Rubin et al. 1980; 11: Márquez & Moles 1996; 12: Amram et al. 1992; 13: Blackman 1977; 14: Rubin et al. 1985; 15: Rubin et al. 1982; 16: Roelfsema & Allen 1985; 17: Afanas'ev 1988b; 18: Rubin et al. 1988; 19: Rhee & Van Albada 1996; 20: Jore 1997; 21: Marcelin et al. 1987.

rather uncertain as well: even the reliability of the distributions derived from numerical simulations of structure formation (e.g. Navarro et al. 1996) is weakened by their apparent discrepancy with the observed RC's of low surface brightness galaxies. Since in this paper we are mainly interested in the properties of bulges and disks, the choice of the dark halo distribution is not likely to be important, at least as long as the visible matter dominates the mass distribution in the inner galaxy regions.

To have an idea of how the fit to the RC is influenced by the inclusion in the model galaxy of a dark component, we perform two different fits for each RC: one using only bulge and disk, and one including also the contribution from a dark halo. The expressions for the rotational velocity of an exponential disk and a generic ellipsoidal bulge are reported in Moriondo et al. (1998c), as well as two possible dark halo distributions, namely a constant density sphere and a pseudo-isothermal one (Kent,

Table 2. The photometric parameters

Name (1)	μ_e (2)	R_e (kpc) (3)	ϵ_b (4)	$\mu(0)$ (5)	R_d (kpc) (6)	i (deg) (7)	\mathcal{M}_H (8)
UGC 00014	16.45 (0.10)	0.66 (0.04)	0.27 (0.01)	17.76 (0.08)	4.08 (0.18)	44.0 (1.9)	-24.03 (0.11)
UGC 00026	17.93 (0.11)	0.94 (0.05)	0.16 (0.02)	19.51 (0.11)	5.69 (0.34)	55.9 (1.2)	-23.14 (0.13)
UGC 00089	14.99 (0.10)	0.75 (0.03)	0.31 (0.02)	16.72 (0.10)	2.79 (0.12)	56.0 (0.5)	-24.63 (0.08)
UGC 00673	18.10 (0.64)	1.92 (0.67)	58.7 (4.3)	-22.27 (0.94)
UGC 00725	18.55 (0.33)	0.35 (0.09)	0.01 (0.23)	18.20 (0.24)	3.40 (0.30)	76.9 (0.3)	-23.00 (0.17)
UGC 00732	17.91 (0.23)	0.40 (0.06)	0.41 (0.01)	17.84 (0.10)	2.85 (0.12)	55.2 (0.6)	-23.02 (0.08)
UGC 00820	16.00 (0.26)	0.81 (0.05)	0.22 (0.01)	16.82 (0.25)	2.85 (0.18)	67.0 (0.5)	-24.50 (0.23)
UGC 00927	16.92 (0.13)	0.29 (0.03)	0.12 (0.08)	18.03 (0.09)	3.83 (0.15)	54.8 (0.5)	-23.44 (0.07)
UGC 00940	19.14 (0.21)	0.68 (0.12)	0.15 (0.17)	18.86 (0.10)	4.16 (0.20)	49.2 (1.7)	-22.86 (0.11)
UGC 00975	17.84 (0.09)	1.73 (0.06)	52.4 (0.7)	-21.96 (0.07)
UGC 01013	15.84 (0.14)	1.14 (0.06)	0.43 (0.01)	17.74 (0.13)	4.74 (0.25)	61.4 (0.5)	-24.69 (0.10)
UGC 01033	17.56 (0.38)	1.15 (0.17)	0.75 (0.01)	18.53 (0.36)	2.87 (0.38)	81.3 (0.4)	-22.82 (0.33)
UGC 01094	17.03 (0.23)	0.66 (0.07)	0.23 (0.04)	17.50 (0.21)	3.40 (0.28)	74.3 (0.3)	-24.21 (0.15)
UGC 01238	16.53 (0.22)	0.85 (0.02)	0.14 (0.01)	18.08 (0.22)	3.02 (0.11)	42.3 (1.4)	-23.38 (0.23)
UGC 01302	15.19 (0.16)	0.32 (0.04)	0.29 (0.07)	17.48 (0.14)	2.41 (0.15)	63.4 (0.9)	-23.39 (0.12)
UGC 01350	17.35 (0.23)	0.94 (0.03)	0.35 (0.01)	18.34 (0.23)	6.15 (0.22)	51.1 (0.6)	-24.25 (0.22)
UGC 01437	15.92 (0.09)	0.54 (0.02)	0.28 (0.01)	16.39 (0.07)	2.64 (0.07)	45.1 (0.7)	-24.37 (0.06)
UGC 01633	16.26 (0.16)	0.47 (0.03)	0.42 (0.05)	16.63 (0.13)	2.76 (0.14)	61.6 (0.3)	-24.22 (0.10)
UGC 01835	17.19 (0.12)	0.75 (0.06)	0.06 (0.01)	17.80 (0.09)	4.32 (0.23)	49.8 (1.6)	-23.95 (0.12)
UGC 01935	14.97 (0.21)	0.50 (0.04)	0.43 (0.02)	17.18 (0.19)	4.33 (0.33)	72.3 (0.3)	-24.88 (0.13)
UGC 01937	16.54 (0.18)	0.58 (0.05)	0.32 (0.06)	16.97 (0.17)	3.13 (0.12)	52.3 (0.8)	-24.20 (0.16)
UGC 02134	17.51 (0.17)	0.95 (0.08)	0.15 (0.05)	17.81 (0.16)	4.15 (0.31)	66.4 (0.9)	-23.89 (0.15)
UGC 02142	15.57 (0.25)	1.01 (0.05)	0.42 (0.01)	17.79 (0.24)	4.64 (0.25)	61.6 (0.5)	-24.58 (0.23)
UGC 02185	17.17 (0.29)	0.22 (0.04)	0.16 (0.19)	17.81 (0.21)	3.64 (0.30)	74.8 (0.3)	-23.56 (0.14)
UGC 02223	19.67 (0.77)	0.40 (0.34)	0.00 (0.86)	18.26 (0.30)	2.76 (0.29)	74.3 (0.9)	-22.51 (0.29)
UGC 02241	17.75 (0.23)	1.93 (0.15)	0.20 (0.03)	18.24 (0.36)	4.20 (0.66)	50.7 (2.8)	-23.93 (0.47)
UGC 02617	17.69 (0.20)	0.52 (0.09)	0.38 (0.14)	18.20 (0.13)	3.16 (0.20)	60.9 (1.1)	-22.88 (0.13)
UGC 02655	18.65 (0.15)	1.93 (0.27)	0.15 (0.07)	18.97 (0.26)	6.26 (1.07)	62.6 (2.7)	-23.64 (0.40)
UGC 02885	15.80 (0.17)	0.69 (0.05)	0.00 (0.04)	17.96 (0.15)	9.42 (0.59)	67.0 (0.4)	-25.58 (0.10)
UGC 11973	16.90 (0.29)	0.35 (0.05)	0.27 (0.16)	16.84 (0.20)	3.61 (0.27)	72.4 (0.3)	-24.57 (0.14)
UGC 12173	17.36 (0.26)	0.38 (0.09)	0.13 (0.25)	17.80 (0.08)	4.59 (0.19)	49.4 (1.4)	-24.02 (0.08)
UGC 12230	17.34 (0.17)	0.49 (0.09)	0.00 (0.14)	17.00 (0.11)	3.10 (0.15)	57.9 (0.7)	-24.01 (0.09)
UGC 12378	17.14 (0.17)	0.42 (0.07)	0.19 (0.18)	17.51 (0.10)	3.40 (0.15)	54.9 (1.0)	-23.77 (0.08)
UGC 12486	15.74 (0.11)	0.66 (0.03)	0.00 (0.02)	17.92 (0.11)	4.04 (0.22)	56.8 (1.1)	-24.12 (0.11)
UGC 12539	16.71 (0.17)	0.32 (0.02)	0.23 (0.04)	17.10 (0.16)	2.12 (0.12)	64.7 (0.3)	-23.17 (0.12)
UGC 12598	16.24 (0.15)	0.23 (0.03)	0.16 (0.10)	16.22 (0.11)	1.43 (0.06)	58.6 (0.4)	-23.18 (0.08)
UGC 12618	15.49 (0.97)	0.65 (0.03)	0.03 (0.05)	16.81 (0.98)	2.01 (0.08)	22.6 (3.8)	-23.83 (0.98)
UGC 12666	19.32 (0.24)	1.46 (0.25)	0.33 (0.08)	19.60 (0.27)	6.97 (1.70)	74.3 (2.4)	-23.14 (0.51)
UGC 12667	17.73 (0.29)	0.28 (0.06)	0.38 (0.01)	17.94 (0.09)	2.84 (0.13)	53.1 (1.2)	-22.82 (0.08)
UGC 12780	16.14 (0.05)	0.61 (0.03)	0.06 (0.05)	17.23 (0.05)	4.75 (0.11)	39.8 (0.7)	-24.81 (0.04)

Notes: Col 2.: bulge effective surface brightness, in mag arcsec⁻². Col. 3: bulge effective radius. Col. 4: bulge ellipticity. Col. 5: disk central surface brightness in mag arcsec⁻². Col 6: disk scalelength. Col. 7: disk inclination. Col. 8: Total absolute magnitude.

1986). The first halo distribution yields a linearly rising RC, and is an approximation of the latter as R tends to zero; the rotation velocity associated to the pseudo-isothermal sphere, on the other hand, tends to a constant value as R goes to infinity. This last distribution has been considered only for the 4 galaxies whose RC is well sampled in the outer, flat part (if this is not the case, and the asymptotic rotation velocity is not well defined, usually the two types of dark matter halos yield the same result, in the sense that only the linear part of the isothermal sphere is used by the minimization routine that fits the data).

In general we find that if a dark component is included in the fit, it never turns out to be dominant in the inner part of the RC, within two disk scalelengths; this is also true when the dark matter distribution is well constrained by a very extended RC. In other words, the solutions we obtain are usually not very different from the “maximum disk” ones, implying that, in most cases, the visible part of the galaxy provides a good match to the observed RC; we will therefore assume that the “maximum disk” hypothesis is basically correct for our galaxies. An alternative scenario, however, will also be considered in Sect. 8. In a few cases the available RC is not extended enough

to constrain even a constant density halo, and in these cases we use the results from the “bulge + disk” fits. We consider these values reliable, since in general the inclusion of the dark halo in the fits does not produce major changes in the estimated mass and M/L of the visible components.

We also note that, in a few cases, at $2.2 R_d$ ’s the contribution to the overall rotation from the bulge is still significant, so that the disk contribution is well below the measured circular velocity. In these cases neglecting the presence of the bulge would certainly lead to overestimate the disk mass and M/L .

Table 3 contains the parameters derived from the RC fits. Also included in the table are the values of the velocity width W (corrected for instrumental smoothing, redshift, turbulence, and inclination), and of the velocity at $2.2 R_d$, V_2 (corrected for redshift and inclination); both quantities will be introduced in the next section. In Fig. 1 (bottom panels) we show the best fits to the RC’s for all the galaxies in our sample.

In 17 cases out of 40, the observed RC has either no data-points in the innermost region (3 cases), or shows no evidence of contribution by the bulge. For these galaxies the bulge mass and M/L are either unconstrained or likely to be underestimated. Most of the 14 galaxies, for which the disk contribution alone is sufficient to match the inner RC, are characterized by the smallest bulge-to-disk ratios (B/D) of the sample ($B/D < 0.05$), or by the faintest bulge luminosities ($\mathcal{M}_b > -21$). It is not surprising, therefore, that in these cases the bulge contribution to the overall RC cannot be adequately resolved. A direct comparison between the M/L of disks and bulges seems to confirm these statements. In Fig. 2 mass versus luminosity is plotted for the disks, and for the bulges with $M_b > 10^9 M_\odot$. These are the 23 cases for which we obtain a reliable fit to the RC for both components, and the two sets of objects seem to form a smooth sequence, roughly delimited by $M/L = 0.25$ and $M/L = 2.5$, in solar units. The remaining “low mass” bulges are placed well below the sequence, out of the plot window, suggesting that their mass is largely underestimated. In the following analysis, therefore, we will consider only the bulges plotted in Fig. 2.

5. The Tully Fisher relation for the sample

To derive an H -band TF relation for our galaxies the 21 cm line velocity widths from the RG and MH database (Table 3) have been corrected for instrumental smoothing, redshift, turbulence, and inclination of the galaxy to the line of sight, according to the prescriptions in Giovanelli et al. (1997, 1998). The absolute galaxy magnitudes in the H band (Table 2) are derived integrating the surface brightness profiles extrapolated up to 8 disk scalelengths; a small correction to face-on aspect is applied, using the results obtained for the disks alone in Moriondo et al. (1998b). Fig. 3 shows the plot we obtain, with the best fit to the data after the exclusion of the three discrepant points to the right. In the case of UGC 12618, our value for the inclination is probably underestimated, leading to an exceedingly large correction for W ; on the other hand, due to its large errorbars, the contribution of this galaxy to the fit is not very significant anyway. In the case of UGC 1350 and UGC 2617, the observed W

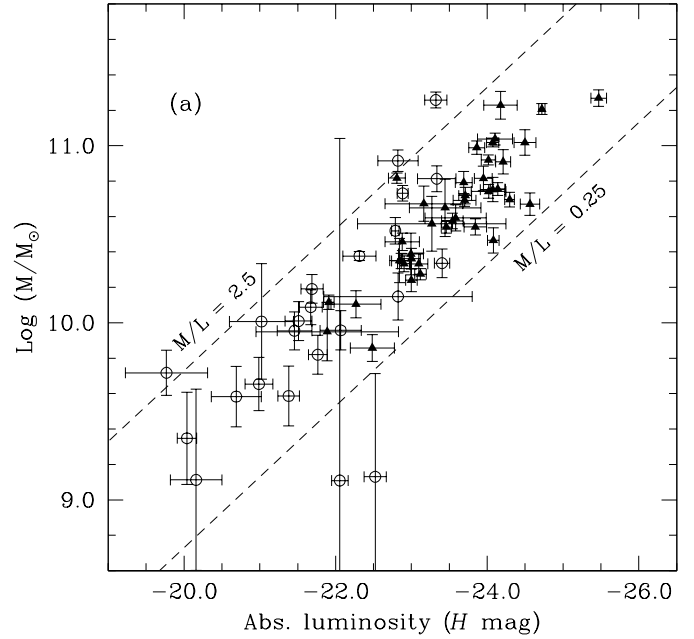


Fig. 2. Mass versus luminosity plotted for bulges and disks of our sample galaxies. Open circles represent the bulges, whereas filled triangles represent the disks. Only bulges with mass $> 10^9 M_\odot$ are plotted. The slope of the two dashed line is of constant M/L . The two M/L values plotted, 2.5 and 0.25, are in solar units (H band).

is likely to be overestimated, maybe for a misidentification of the galaxy; we note that for these two objects an estimate of the rotation derived from the RC is, respectively, about 75% and 50% smaller than W .

The errors on both axes are of comparable magnitude, therefore the weight for each data point is the RMS of the two contributions. Since the relation we fit is $y = ax + b$, the i -th residual is weighted by

$$w(i) = \left[\sqrt{\epsilon_{y(i)}^2 + a^2 \epsilon_{x(i)}^2} \right]^{-1}, \quad (2)$$

where the ϵ ’s are the estimated errors. The slope and zero offset, with respect to the average $\log W$, are respectively -7.7 ± 1.0 and -23.67 ± 0.08 .

6. Fundamental planes

We now fit separately to bulges and disks a relation

$$\log R = a \log V + b \log I + c \quad (3)$$

involving a scalelength, a velocity, and a surface brightness, analogous to the FP of elliptical galaxies. The designated parameters for the bulges are the effective radius R_e , the surface brightness at R_e (I_e), and a velocity defined as

$$V_b = \sqrt{\frac{M_b}{R_e}} \quad (4)$$

where M_b is the bulge mass, in units of $10^9 M_\odot$. Since for all the bulges selected (the ones with $M_b > 1$) the brightness distribution is fitted by a pure exponential – i.e. they all have the

Table 3. The dynamical parameters

Name (1)	M_b (2)	$(M/L)_b$ (3)	M_d (4)	$(M/L)_d$ (5)	W (km s $^{-1}$) (6)	v_2 (km s $^{-1}$) (7)
UGC 00014	12.2 (3.0)	0.95 (0.25)	97.5 (9.4)	1.25 (0.16)	456.7 (18.0)	215.0 (18.2)
UGC 00026	22.5 (7.0)	0.74 (0.25)	271.6 (5.8)	90.0 (27.6)
UGC 00089	21.7 (4.4)	0.34 (0.08)	29.2 (5.2)	0.31 (0.06)	445.2 (5.5)	180.0 (31.2)
UGC 00673	8.9 (3.7)	0.70 (0.53)	299.2 (15.1)	120.0 (26.0)
UGC 00725	24.5 (7.2)	0.68 (0.26)	293.1 (8.2)	160.0 (44.9)
UGC 00732	17.4 (2.8)	0.49 (0.09)	289.7 (24.4)	120.0 (18.7)
UGC 00820	55.1 (5.3)	0.61 (0.16)	462.7 (4.9)	240.0 (17.4)
UGC 00927	34.7 (2.9)	0.64 (0.08)	314.3 (35.0)	150.0 (11.2)
UGC 00940	65.7 (4.8)	2.22 (0.27)	328.8 (15.7)	160.0 (8.9)
UGC 00975	13.1 (1.3)	1.01 (0.13)	275.0 (6.8)	128.0 (12.0)
UGC 01013	181.1 (20.1)	2.64 (0.46)	81.1 (14.0)	0.75 (0.16)	550.9 (5.5)	300.0 (49.5)
UGC 01033	10.2 (8.3)	0.72 (0.64)	12.7 (2.4)	0.67 (0.28)	323.1 (3.3)	160.0 (22.0)
UGC 01094	3.9 (1.6)	0.51 (0.25)	49.2 (4.3)	0.71 (0.16)	435.2 (4.5)	212.0 (5.6)
UGC 01238	23.8 (1.5)	1.18 (0.27)	28.7 (3.5)	0.91 (0.23)	397.9 (12.6)	180.0 (21.1)
UGC 01302	9.0 (2.4)	0.92 (0.29)	23.1 (3.3)	0.65 (0.13)	353.9 (5.3)	190.0 (24.8)
UGC 01350	169.2 (33.2)	1.63 (0.49)	731.3 (27.2)	240.0 (46.2)
UGC 01437	6.6 (1.8)	0.46 (0.13)	49.6 (5.2)	0.43 (0.05)	420.1 (7.5)	205.0 (20.6)
UGC 01633	4.5 (1.7)	0.58 (0.24)	56.9 (5.2)	0.56 (0.09)	479.4 (6.4)	240.0 (18.3)
UGC 01835	10.2 (2.8)	1.20 (0.36)	65.4 (11.4)	0.77 (0.15)	423.2 (11.7)	207.0 (34.2)
UGC 01935	1.4 (2.0)	0.05 (0.07)	46.8 (7.4)	0.31 (0.08)	447.0 (3.5)	200.0 (27.8)
UGC 01937	56.5 (9.7)	0.60 (0.14)	437.8 (6.6)	200.0 (33.5)
UGC 02134	15.5 (3.1)	1.56 (0.41)	34.8 (4.0)	0.45 (0.09)	335.6 (4.4)	160.0 (13.9)
UGC 02142	65.1 (11.8)	0.95 (0.29)	109.2 (9.2)	1.12 (0.29)	520.1 (5.2)	250.0 (16.3)
UGC 02185	37.6 (4.1)	0.63 (0.15)	437.1 (14.9)	200.0 (14.2)
UGC 02223	7.2 (1.3)	0.32 (0.11)	244.9 (10.2)	125.0 (19.5)
UGC 02241	82.3 (12.5)	2.46 (0.68)	44.6 (18.0)	0.84 (0.45)	461.9 (20.4)	250.0 (93.0)
UGC 02617	22.4 (2.4)	0.72 (0.12)	535.4 (19.7)	138.0 (12.0)
UGC 02655	9.1 (2.5)	0.62 (0.20)	39.1 (7.2)	0.65 (0.20)	307.0 (20.0)	140.0 (10.2)
UGC 02885	53.8 (5.9)	2.12 (0.43)	185.7 (21.7)	0.54 (0.10)	...	280.0 (27.6)
UGC 11973	104.1 (18.7)	0.73 (0.20)	503.2 (5.9)	360.0 (59.1)
UGC 12173	5.2 (1.7)	2.80 (1.16)	104.2 (6.4)	1.10 (0.11)	465.3 (12.6)	210.0 (9.7)
UGC 12230	83.1 (5.8)	0.92 (0.12)	517.0 (8.5)	260.0 (12.9)
UGC 12378	1.3 (1.7)	0.47 (0.60)	52.3 (6.1)	0.77 (0.12)	407.4 (6.6)	200.0 (21.5)
UGC 12486	33.1 (6.2)	1.32 (0.29)	61.9 (9.6)	0.93 (0.18)	432.6 (7.1)	210.0 (30.5)
UGC 12539	2.2 (1.5)	0.92 (0.62)	21.5 (3.3)	0.56 (0.12)	375.2 (5.3)	160.0 (22.5)
UGC 12598	18.8 (1.5)	0.48 (0.06)	360.2 (4.0)	170.0 (11.0)
UGC 12618	14.1 (4.7)	0.47 (0.48)	36.2 (14.0)	0.80 (0.84)	630.9 (105.4)	215.0 (82.6)
UGC 12666	3.8 (1.6)	0.84 (0.41)	47.0 (11.7)	1.12 (0.41)	271.9 (5.5)	150.0 (7.1)
UGC 12667	21.5 (2.4)	0.67 (0.09)	253.7 (6.0)	140.0 (14.2)
UGC 12780	1.3 (6.2)	0.09 (0.42)	161.0 (12.2)	0.94 (0.08)	515.8 (10.0)	260.0 (18.9)

Notes: Cols. 2,4: masses in units of $10^9 M_\odot$. Cols. 3,5: M/L's in solar units.

same shape – this velocity scales as the rotation velocity, measured at 2.2 bulge scalelengths R_b . Also, R_e and I_e are related by constant factors respectively to R_b and the central surface brightness $I(0)$ (the two parameters usually adopted for the disks): $R_e = 1.67 R_b$, and $I_e = 0.19 I(0)$. For the disks we choose the exponential scalelength R_d , the central surface brightness $I(0)$, and a velocity V_d defined via a relation analogous to Eq. (4), with the disk mass and the disk scalelength. Again, this velocity differs from the value at $2.2 R_d$ by the same factor for all the exponential distributions. Following CY95, we also consider a relation involving R_d , $I(0)$, and the *total galaxy*

rotation velocity at $2.2 R_d$, derived directly from the RC, which we will indicate as V_2 .

It turns out that the three parameters to be fitted have comparable uncertainties, and each point needs to be weighted by a combination of them. In the case of the structural parameters (R , I), besides the formal error from the fit to the brightness distributions, a major contribution is added from the errors in the corrections to face-on aspect, that is from the uncertainty in the amount of internal extinction. These are evaluated according to the results in Moriondo et al. (1998b). The uncertainty on the velocity depends in principle on the errors associated both to the RC measurement and to the scale length. However we ex-

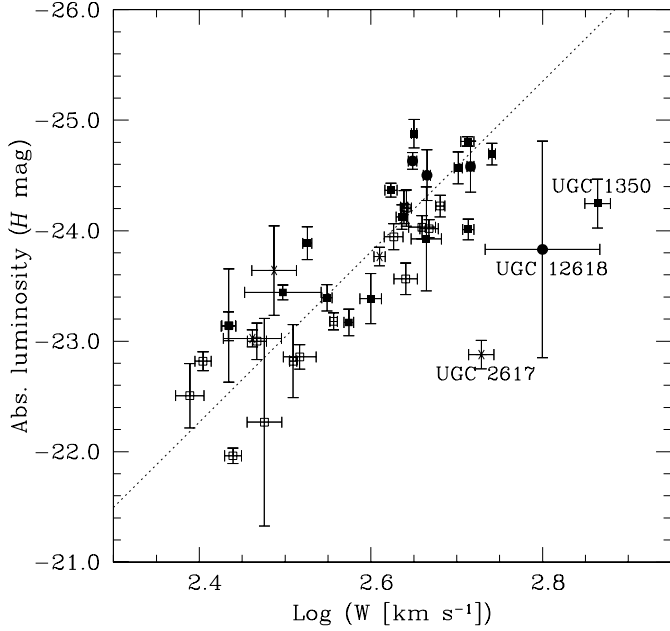


Fig. 3. The H -band Tully-Fisher relation for our sample, with the best fit to the data after the exclusion of the three discrepant points on the right side. Different symbols correspond to different morphological types: filled circles for Sa-Sab, filled squares for Sb-Sbc, open squares for Sc-Scd, crosses for Sd and dm.

pect this latter contribution to be less important, especially for the disks, whose scalelength is always the best determined parameter in the surface brightness decompositions. Therefore we assume the uncertainty on the velocities to be well represented by the formal error derived from the fitting routine. The errors on all other quantities are derived from these values: for example, the error on the disk mass is obtained combining the uncertainties on the velocity and the scale length, since $M \sim v^2 R$.

The fit to the disk parameters yields

$$\log R_d = (1.31 \pm 0.19) (\log V_d - \langle \log V_d \rangle) + (-0.62 \pm 0.09) (\log I(0) - \langle \log I(0) \rangle) + (1.29 \pm 0.07) , \quad (5)$$

where “ $\langle \rangle$ ” designates the average over the sample. If V_2 is chosen, instead of the value defined in terms of the disk mass and scalelength, we obtain

$$\log R_d = (1.47 \pm 0.16) (\log V_2 - \langle \log V_2 \rangle) + (-0.61 \pm 0.07) (\log I(0) - \langle \log I(0) \rangle) + (1.39 \pm 0.06) . \quad (6)$$

We note that these coefficients are close to the values implied by the TF relation derived in Sect. 5: in fact, from $L \sim W^{3.1}$, we derive $R \sim W^{1.5} I^{-0.5}$. Therefore, the TF relation is a nearly edge-on projection of the FP. Also, these values are not inconsistent with the constraint implicit in the relation suggested by CY95 (Eq. (1)), i.e. $a = 2b$.

The best fit to the bulge parameters yields:

$$\log R_e = (0.97 \pm 0.13) (\log V_b - \langle \log V_b \rangle) + (-0.61 \pm 0.08) (\log I_e - \langle \log I_e \rangle) + (-0.46 \pm 0.10) . \quad (7)$$

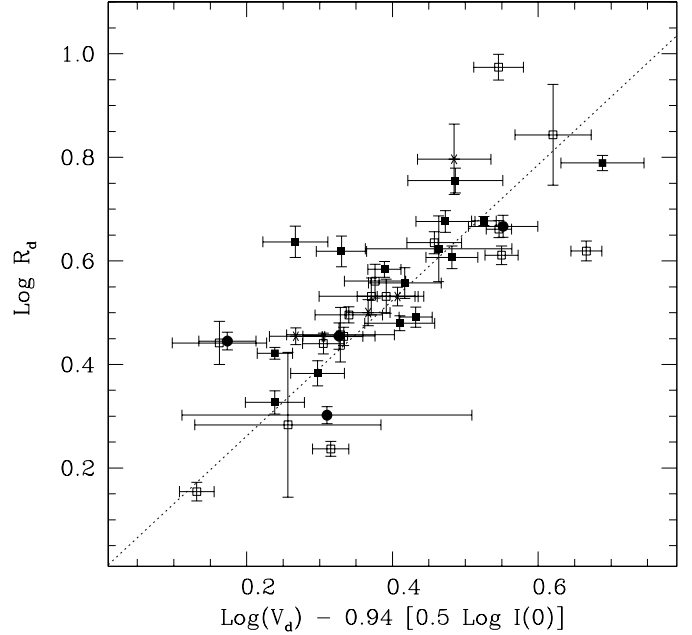


Fig. 4. The scaling relation of Eq. (5) for the disks, derived from the best fit to the RC. The data and the best fit are shown. The factorization of the $I(0)$ coefficient in the x -axis label is chosen to make it easily comparable with Eq. (1). Symbols are as in Fig. 3.

Again, a relation like Eq. (1) is not ruled out, even if with a slope a slightly different from the disks’ value.

The errors associated to the various coefficients are estimated by performing a large number of Monte Carlo simulations of the data sample and fitting each simulation, to derive a distribution of values for each coefficient. Figs. 4 and 5 show the relations we find for the disks, whereas Fig. 6 shows the one for the bulges.

6.1. A comparison with published results

The coefficients we derive for the disks are different from the values found by CY95 ($a = 1.0$, $b = -0.5$), but closer to the ones reported by Karachentsev (1989), i.e. $a = 1.4$, $b = -0.7$; we note however that, in the case of CY95, the photometric data were in a very different passband (B). Both our coefficients and the other quoted values are not consistent with what would be expected on the basis of the virial theorem and a universal mass-to-light ratio ($a = 2$ and $b = -1$).

The various sets of coefficients can also be compared to the ones which define the FP of elliptical galaxies, evaluated using the central velocity dispersion as the kinematic parameter, and the effective surface brightness. For example, Bender et al. (1992) report for the Virgo cluster $a = 1.4$ and $b = -0.85$, in the B band; more recently Jørgensen et al. (1996) find $a = 1.24$ and $b = -0.82$ in the Gunn r band, with a scatter of 0.084 in $\log R_e$; Pahre et al. (1998a) estimate the NIR coefficients of the plane to be $a = 1.53$ and $b = -0.79$. The various FP’s are not very different, and actually the existence of a “cosmic metaplane” has already been claimed by Bender et al. (1997), and BBFN. In par-

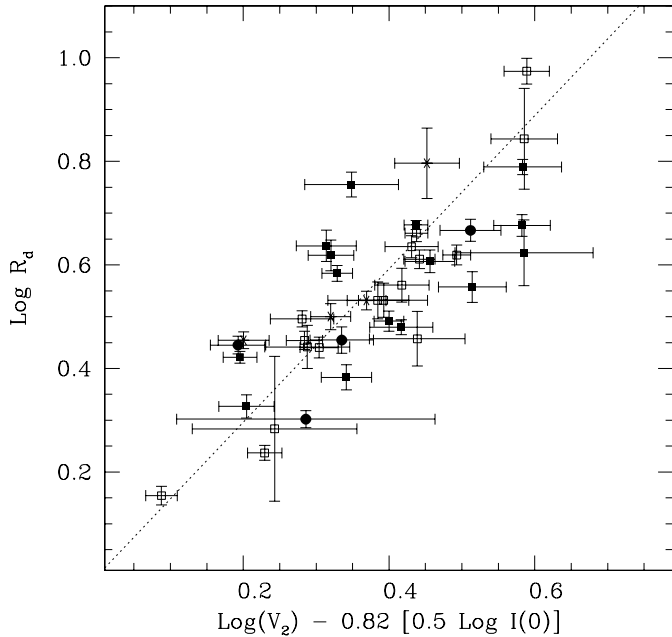


Fig. 5. The scaling relation of Eq. (6) for the disks, derived using the rotation velocities at $2.2 R_d$. The data and the best fit are shown. Symbols as in Fig. 3.

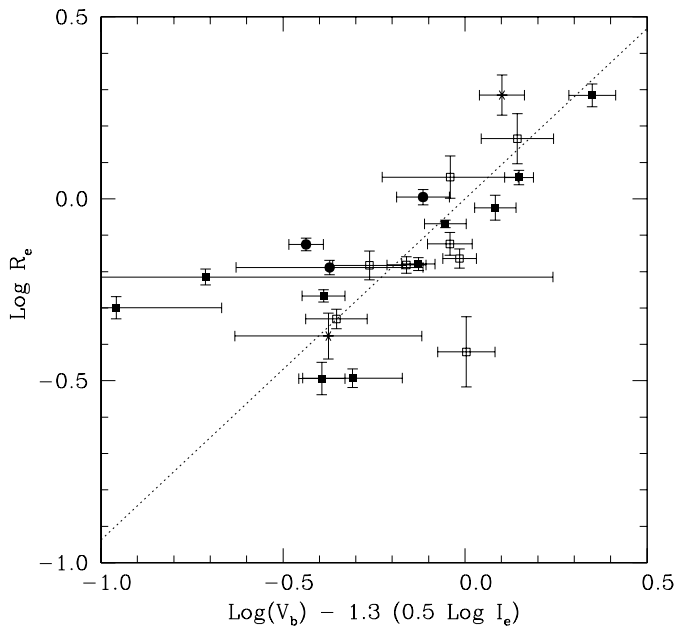


Fig. 6. The scaling relation of Eq. (7) for the bulges. The data and the best fit are shown. Symbols as in Fig. 3.

particular they defined a set of three parameters (the k parameters) particularly suited to represent the FP of elliptical galaxies in the B band, and found that basically all the self-gravitating systems show a similar behaviour in the k -parameter space. In the case of spiral galaxies, they considered their global properties, without attempting a decomposition into structural components, and for the bulges in their data sample they used the central velocity dispersion as the kinematical parameter. This work improves

the approach by characterizing separately bulges and disks from the photometric point of view; in addition, we are able to determine the bulge mass independently of its kinematical status (i.e., if it's more or less supported by rotation), and obtain an independent estimate of the coefficients of the bulge FP.

Fig. 7 shows our data in the H -band k -space, with bulges denoted as open circles, and disks as triangles. We have defined the three coordinates as $k_1 = \log(M)$, $k_2 = \log(M/L \cdot I_e^3)$, and $k_3 = \log(M/L)$, where M is the total mass in units of M_\odot , M/L is the stellar mass-to-light ratio in solar units, and I_e is the effective surface brightness in $L_\odot pc^{-2}$. These definitions, besides being applied to a different passband, are slightly different from the ones introduced by Bender et al. (1992). We can calculate the transformations between the two sets of coordinates from the relations reported in the Appendix A to BBFN, and assuming that all our bulges and disks are adequately described by exponentials. Using a typical $B - H = 3.5$ for both components, we find

$$\begin{cases} k_1^B = \frac{1}{\sqrt{2}} (k_1 - 5.97) \\ k_2^B = \frac{1}{\sqrt{6}} (k_2 + 0.58) \\ k_3^B = \frac{1}{\sqrt{3}} (k_3 + 1.37) \end{cases} \quad (8)$$

where k_1^B , k_2^B , and k_3^B are the B -band BBFN parameters.

The dotted line in the upper right corner of the k_1 vs. k_2 plot corresponds, in our set of coordinates, to the boundary of the so-called Zone of Exclusion (ZOE), defined in the B band by $k_1^B + k_2^B > 8$: it is consistent with our data, in the sense that most bulges and all the disks are placed to its left side. The BBFN database for the bulges is here extended to lower masses, with several data-points falling in the typical range of dwarf ellipticals ($M < 10^{10} M_\odot$); the two classes of objects appear however separated, with the bulges shifted towards higher values of k_2 , and therefore higher concentrations (note that, for a given mass, k_2 is proportional to $\log(I_e^2/R_e^2)$, which is higher for compact, bright objects).

For what concerns spiral galaxies, BBFN find that their average distance from the ZOE increases steadily with morphological type, from Sa's to Irregulars; the data points of our disks, however, are all placed in about the same region of the k_1 - k_2 plane, quite distant from the ZOE, and roughly coincident with the locus occupied by Scd's galaxies in the BBFN's plots. Most likely, this difference arises from the separation of the two structural components, which has allowed us to plot the k parameters of the *disks alone*: if the values for the whole galaxies are considered, one would expect the systems with higher B/D (namely, the early-type spirals) to lie closer to the ZOE, due to the contamination of the bulge. The BBFN sequence, therefore, would be mainly driven by the average B/D , which in turn is roughly correlated with morphological type. When considered separately, on the other hand, disks and bulges are located in two distinct, contiguous regions of the k -space, as it is also evident from the k_2 - k_3 projection, with the disks shifted towards higher masses and lower concentrations. A different ZOE could in principle be defined for the disks, with about the same slope but shifted by about two decades towards lower k_2 values.

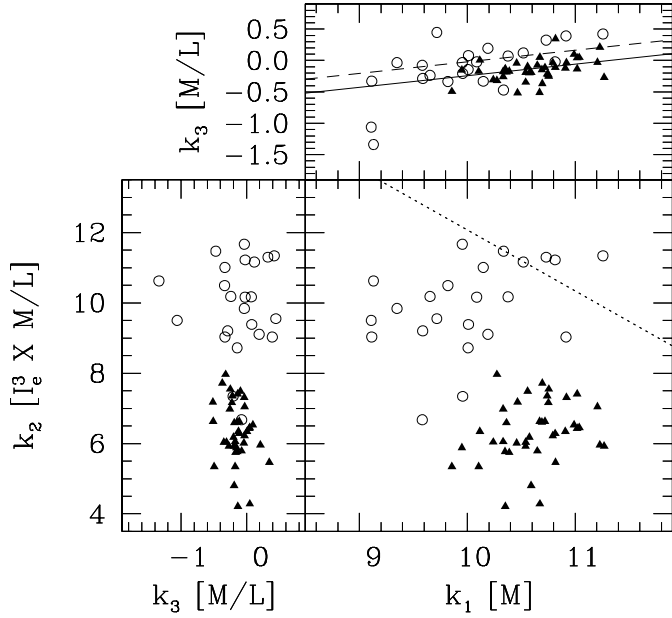


Fig. 7. Bulges (open circles) and disks (triangles) in the k -space defined by Bender et al. (1992). In the top panel the slope of the FP for elliptical galaxies is plotted for comparison. In the k_1 versus k_2 panel the dotted line represents the Zone of Exclusion, as defined by BBFN.

In the top panel of Fig. 7, we have plotted the slope of the B -band FP for the Virgo cluster, scaled to the centroid of the bulges (dashed line) and of the disks (solid line). It appears to be consistent with our data, as suggested by the similarity of our coefficients in Eqs. (5) and (6) to the ones reported by Bender et al. (1992). Also, using Eqs. (8) and the definition in BBFN, we can estimate the quantity $\delta_{3:1}$ for bulges and disks, representing their average vertical distance from the ellipticals' FP in the $k_1^B - k_3^B$ projection. In the case of the bulges, we find $\delta_{3:1} = 0.03$ dex, in fair agreement with the BBFN estimate (-0.03); for the disks we find a shift of -0.19 dex, which is about the value found by BBFN for spirals from type Sa to Sc.

7. The disk FP as a distance indicator

In order to assess the goodness of Eqs. (5) and (6) as tools to measure galaxy distances, we compare the scatter of the data points, with respect to the best fit, to the scatter associated to the TF relation. The dispersion is defined as

$$\sigma = \sqrt{\frac{\sum_i (\Delta_i w_i)^2}{\sum_i w_i^2}},$$

where Δ_i is the residual on the i -th data point and w_i the associated weight, defined by Eq. (2). We find a dispersion of 0.38 mag for the TF relation, implying an uncertainty of 19% on the distance of a single galaxy. We note that the galaxy distances used in this context have been estimated purely from redshifts. The peculiar velocity field thus adds scatter to the corresponding TF relation in a measure which we estimate on the order of 0.15 to 0.20 mag, at the typical distance of these objects. Had peculiar velocity-corrected distances been used, the TF scatter would

have been so that distance estimates would have uncertainties of about 16%, rather than 19%.

In the case of the FP, we find a dispersion of 0.11 in $\log r$ if we use velocities derived from the best fits (Eq. (5)), and of 0.09 if the velocities are the actual rotation velocities (Eq. (6)). The associated uncertainties in the distance are respectively about 29% and 23%. Even if these two values are less than 1/2 of the dispersion quoted by Giovanelli for the relation proposed by CY95 and a sample of 153 spiral galaxies (0.25 in $\log r$, not based on a detailed disk-bulge decomposition analysis as we use here), they are still larger than the uncertainty yielded by the TF relation for our sample. Therefore, according to our data, the disk FP is not as accurate, as a distance indicator, as the TF relation, even if it allows for one more free parameter in the relation. This result could be imputed to the scatter added to the relation by the uncertainties introduced in the data analysis process (in particular, the decomposition of the surface brightness distribution and the fit to the RC). On the other hand, we find that a modified Tully-Fisher relation, in which the velocity width is replaced by V_2 , is characterized as well by a larger dispersion of 0.45 mag. This value is equivalent to the dispersion of 0.09 in $\log r$ associated to Eq. (6). In a similar way, if the total luminosity is replaced by the luminosity within $2.2 R_d$'s, we find a very large dispersion of 0.64 mag. Since these alternative parameters are not strictly derived from the surface brightness decompositions or by the fit to the RC's, as it is the case for the FP ones, we argue that using parameters associated with the inner part of the galaxy (rather than global quantities), is in itself a major source of scatter in the scaling relation considered. Thus, the fine tuning between photometric and kinematic parameters that yield the TF relation would be more effective because of their global character. About the much reduced dispersion with respect to the Giovanelli data, we attribute this difference to the use of a more refined data-analysis technique for our sample.

8. The relation between mass and luminosity

Eqs. (5)–(7) show that for both disks and bulges a systematic variation of M/L exists, if we assume that we have properly evaluated their shape, photometric properties (including the effect of internal extinction), and contribution to the RC. In particular we can rewrite Eqs. (5) and (7) as

$$L_d \sim \frac{M_d^{1.0 \pm 0.2}}{R_d^{0.7 \pm 0.4}} \quad (9)$$

and

$$L_b \sim \frac{M_b^{0.8 \pm 0.2}}{R_e^{0.5 \pm 0.3}}. \quad (10)$$

Whereas for elliptical galaxies the $M - L$ plane shows an edge-on view of the FP, this is not the case for disks and bulges, and a residual dependence on the scalelength is left; this dependence is such that, if a given mass settles into a larger size, the corresponding M/L ratio is larger. Actually, this result is already implicit in the work by CY95: a good match to Eq. 1 with $a \neq 2$ is possible only if M/L is a function of R_d alone.

Previous results, both observational (Persic et al. 1996), and theoretical (Navarro et al. 1996, Navarro 1998), have suggested that the stellar M/L in the B band increases with the galaxy luminosity, rather than with its size. This conclusion is probably consistent with ours, since the total galaxy luminosity, especially in the B band, is mainly determined by the disk scalelength. Since the average stellar M/L ratios are determined by the star-formation history of the galaxy, a connection must necessarily exist between the structural properties of the system, in particular its size, and the characteristics of its average stellar population. This is not surprising, since connections of this kind also exist for elliptical galaxies: for example the one at the base of the well-known color-magnitude relation. On the other hand, the parameters which characterize stellar populations (age, metallicity, star-formation rate, etc.), whose systematic variation could be responsible of the observed trend, are far too many to be constrained by our H -band data alone. Some additional information on this issue could be provided by a detailed multiband analysis – possibly integrated by spectroscopic data – as the one recently carried out by Pahre et al. (1998b) for elliptical galaxies.

We note however that a different scenario can be outlined, in particular if we forget Eqs. (9) and (10), and assume instead that the stellar M/L ratio is constant for all the galaxies. In this hypothesis, Eq. (6) can be used to predict how the contribution of the disk to the RC should scale with surface brightness and scalelength. Since we have, for an exponential disk:

$$V_d \sim [(M/L) I(0) R_d]^{0.5}, \quad (11)$$

and from Eq. (6):

$$V_2 \sim I(0)^{0.41} R_d^{0.68},$$

if M/L is a constant, we derive

$$\frac{V_d}{V_2} \sim \frac{I(0)^{0.09 \pm 0.07}}{R_d^{0.18 \pm 0.07}}, \quad (12)$$

implying that the relative disk contribution to the RC should be the smallest for large galaxies and, although with less significance, for low surface brightness ones¹. For the bulges, using Eqs. (7) and (11), we find a trend with size similar to the one expressed by Eq. (12). Considering the range of parameters, rather uniformly covered by our sample (about three magnitudes in $I(0)$ and a factor of 4 in R_d), and assuming that the brightest and more compact disks contribute about 90% to the overall RC at $2.2 R_d$, then Eq. (12) implies that, for the galaxies with the largest radii and faintest surface brightness, V_d should be about 55% of the observed rotation velocity. In this hypothesis a “maximum disk” RC can be ruled out in most cases; of course, to match the observed RC’s, we have to postulate a conspicuous increase with size of the relative amount of dark matter. As already mentioned in Sect. 4, the results by Bottema (1993,

1997) and by Courteau & Rix (1999) support a scenario of this kind, with the disk contributing, on average, about 60% of the rotation at $2.2 R_d$ ’s. Assuming that this rule holds for our sample as well, then, Eq. (12) predicts that the ratio V_d/V_2 should vary throughout the sample between about 0.45 and 0.75, in a well defined way according to the size and surface brightness of each disk. Neglecting the presence of the bulge, and assuming an infinitely thin disk, the corresponding ratio of dark to visible mass within R_2 can be expressed as

$$\frac{M_h}{M_d} \simeq 0.8 \left[\left(\frac{V_2}{V_d} \right)^2 - 1 \right].$$

This quantity changes by more than a factor of 8 in our sample, from 0.4 to 3.3, whereas in the “maximum disk” hypothesis it stays roughly constant: in principle, the predictions of a reliable model for galaxy formation could help to distinguish between two such different behaviours.

Of course, any intermediate scenario between the two extremes discussed here (“maximum disk” solutions and constant stellar M/L) could be considered as well. From the observational point of view, again, more detailed spectrophotometric data might better constrain possible variations in the average stellar population of different galaxies, and help to distinguish between the different possibilities.

9. Summary

Using near-infrared images and rotation curves of a sample of 40 spiral galaxies, we have determined the scaling relations, between structural and kinematic parameters of bulges and disks, analogous to the Fundamental Plane of elliptical galaxies. The accuracy of the disk FP as a distance indicator, for this set of data and our photometric decompositions, is comparable but slightly lower than the one attained by the Tully-Fisher relation. This suggests that the fine tuning between dark and visible components at the basis of the various scaling relations is more effective for global parameters. Also, we deduce that (a) either the stellar mass-to-light ratio of the disk increases with R_d , or (b) the disk contribution to the observed RC decreases according to Eq. (12) for galaxies of large size. A similar behaviour is observed for the bulges.

Acknowledgements. We would like to thank the referee, A. Bosma, for his careful reading of the manuscript, C. Giovanardi and L. Hunt for insightful comments and suggestions, and Stephane Courteau for having provided his data in electronic format. This research was partially funded by ASI Grant ARS-98-116/22. Partial support during residency of G.M. at Cornell University was obtained via the NSF grant AST96-17069 to R. Giovanelli.

References

- Afanas’ev V.L., Burenkov A.N., Zasov A.V., et al., 1988a, *Astrofizika* 28, 243
- Afanas’ev V.L., Burenkov A.N., Zasov A.V., et al., 1988b, *Astrofizika* 29, 155
- Amram P., Marcelin M., Bonnarel F., et al., 1992, *A&A* 263, 69

¹ From Eqs. (5) and (6) we can see instead that, in our RC fits, the ratio V_d/V_2 is about constant, i.e. independent of R_d and $I(0)$: it amounts to about 85% on average, the typical “maximum disk” value. As a consequence, the disk M/L must increase with R_d .

- Amram P., Marcelin M., Balkowski C., et al., 1994, *A&AS* 103, 5
- Bender R., Burstein D., Faber S.M., 1992, *ApJ* 399, 462
- Bender R., Burstein D., Faber S.M., 1997, In: da Costa, Renzini (eds.) *Proceedings of: Galaxy Scaling Relations: Origins, Evolution and Applications*. Springer-Verlag, p. 95
- Blackman C.P., 1977, *MNRAS* 178, 15
- Bosma A., 1998, *astro-ph/9812013*
- Bottema R., 1993, *A&A* 275, 16
- Bottema R., 1997, *A&A* 328, 517
- Broeils A.H., Van Woerden H., 1994, *A&AS* 107, 129
- Burstein D., Bender R., Faber S.M., et al., 1997, *AJ* 114, 1365 (BBFN)
- Chiba M., Yoshii Y., 1995, *ApJ* 442, 82 (CY95)
- Ciotti L., 1997, In: da Costa, Renzini (eds.) *Proceedings of: Galaxy Scaling Relations: Origins, Evolution and Applications*. Springer-Verlag, p. 38
- Corradi R.L.M., Capaccioli M., 1991, *A&AS* 90, 121
- Courteau S., 1992, Ph.D. Thesis
- Courteau S., Rix H., 1999, *ApJ* 513, 561
- Dalcanton J.J., Spergel D.N., Summers F.J., 1997, *ApJ* 482, 659
- de Blok W.J.G., McGaugh S.S., 1997, *MNRAS* 290, 533
- de Vaucouleurs G., de Vaucouleurs A., Corwin Jr. H.G., et al., 1991, *Third Reference Catalogue of Bright Galaxies*. Springer-Verlag, New York
- Dubinski J., Mihos J.C., Hernquist L., 1999, *astro-ph/9902217*
- Gavazzi G., 1993, *ApJ* 419, 469
- Gavazzi G., 1997, In: da Costa, Renzini (eds.) *Proceedings of: Galaxy Scaling Relations: Origins, Evolution and Applications*. Springer-Verlag, p. 126
- Gerhard O.E., 1999, *astro-ph/9902247*
- Giovanelli R., 1997, In: da Costa, Renzini (eds.) *Proceedings of: Galaxy Scaling Relations: Origins, Evolution and Applications*. Springer-Verlag, p. 146
- Giovanelli R., Haynes M.P., Herter T., et al., 1997, *AJ* 113, 53
- Giovanelli R., Dale D., Haynes M.P., et al., 1998, *AJ*, submitted
- Jore K., 1997, Ph.D. Thesis, Cornell University
- Jørgensen I., Franx M., Kjaergaard P., 1996, *MNRAS*, 280, 167
- Karachentsev I., 1989, *AJ* 97, 1566
- Kent S.M., 1986, *AJ* 91, 1301
- Marcelin M., Lecoarer E., Boulesteix J., et al., 1987, *A&A* 179, 101
- Márquez I., Moles M., 1996, *A&AS* 115, 407
- Martimbeau M., Carignan C., Roy J., 1994, *AJ* 107, 543
- Mathewson D.S., Ford V.L., Buchhorn M., 1992, *ApJS* 81, 413
- Moriondo G., Giovanardi C., Hunt L.K., 1998a, *A&AS* 130, 81
- Moriondo G., Giovanelli R., Haynes M.P., 1998b, *A&A* 338, 795
- Moriondo G., Giovanardi C., Hunt L.K., 1998c, *A&A* 339, 409
- Moriondo G., Baffa C., Casertano S., et al., 1999, *A&AS*, in press
- Navarro J.F., Frenk C.S., White S.D.M., 1996, *AJ* 462, 563
- Navarro J.F., 1998, *astro-ph/9807084*
- Oosterloo T., Shostak S., 1993, *A&AS* 99, 379
- Pahre M.A., Djorgovski S.G., de Carvalho R.R., 1998a, *AJ* 116, 1591
- Pahre M.A., de Carvalho R.R., Djorgovski S.G., 1998b, *AJ* 116, 1606
- Peletier R.F., de Grijs R., 1998, *MNRAS* 300, L3
- Persic M., Salucci P., Stel F., 1996, *MNRAS* 281, 27
- Prugniel P., Zasov A., Busarello G., et al., 1998, *A&AS* 127, 117
- Rhee M.H., van Albada T.S., 1996, *A&AS* 115, 407
- Roelfsema P.R., Allen R.J., 1985, *A&A* 146, 213
- Rubin V.C., Ford W.K., Thonnard N., 1980, *ApJ* 238, 471
- Rubin V.C., Ford W.K., Thonnard N., 1982, *ApJ* 261, 439
- Rubin V.C., Burstein D., Ford W.K., et al., 1985, *ApJ* 289, 81
- Rubin V.C., Whitmore B.C., Ford W.K., 1988, *ApJ* 333, 522
- Scodreggio M., 1997, Ph.D. Thesis, Cornell University
- Sèrsic J.L., 1968, *Atlas de Galaxias Australes*. Observatorio Astronómico, Córdoba
- Szomoru A., Guhathakurta P., van Gorkom J.H., et al., 1994, *AJ* 108, 491
- Tully R.B., Fisher J.R., 1977, *A&A* 54, 661
- Tully R.B., Pierce M.J., Huang J., et al., 1998, *AJ* 115, 2264
- van Albada T.S., Bahcall J.N., Begeman K., et al., 1985, *ApJ* 295, 305
- van Moorsel G.A., 1983, *A&AS* 54, 19
- Verheijen M., Tully B., 1998, *astro-ph/9810297*
- Vogt N.P., 1995, Ph.D. Thesis, Cornell University